A Sterically Congested Nitrogenated Benzodipentaphene with a Double π-Expanded Helicene Structure

Fengkun Chen,[a] Wenting Gu,[b] Akinori Saeki,[b] Manuel Melle-Franco,[c] and Aurelio Mateo-Alonso*[a][d]

[a] POLYMAT, University of the Basque Country UPV/EHU. Avenida de Tolosa 72, 20018 Donostia-San Sebastian (Spain)

[b] Department of Applied Chemistry, Graduate School of Engineering, Osaka University, Suita, Osaka 565-0871 (Japan)

[c] CICECO—Aveiro Institute of Materials. Department of Chemistry, University of Aveiro. 3810-193 Aveiro (Portugal)

[d] Ikerbasque, Basque Foundation for Science, Bilbao (Spain)

KEYWORDS. non-planar aromatics, helical aromatics, π-expanded helicenoids

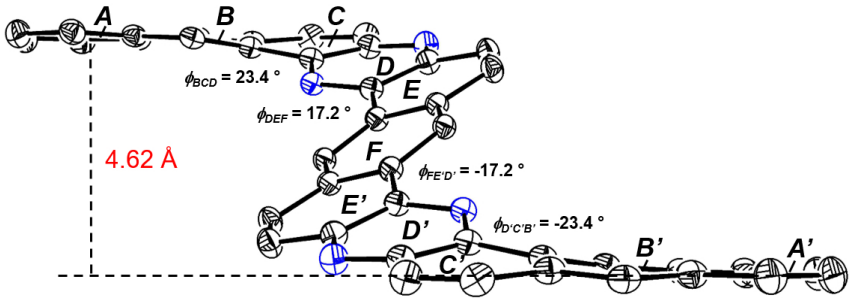

ABSTRACT: Herein, we describe a series of three sterically congested nitrogenated benzodipentaphenes, one of which shows a highly distorted aromatic backbone with an unprecedented double π-expanded helicene structure.

INTRODUCTION

Non-planar polycyclic aromatic hydrocarbons and nanographenes[1] have shown particular optoelectronic and electrochemical properties, enhanced solubility, and unique intermolecular π-contacts in comparison to planar systems. This has stimulated in recent years the synthesis and exploration of increasingly complex aromatics with helical topologies.[2] Among these, helicenes[1h-j] are constituted of angularly *ortho*-annulated rings and exhibit a helical structure along the axis perpendicular to the rings, as the result of the steric interactions between aromatic rings or their substituents (Figure 1a). Helicenes have received considerable attention both as synthetic challenges and as functional materials for several applications, which include polarized light emission and detection,[3] non-linear optics,[4] electronics,[3e,5] and spintronics.[3e,6]

There is an emerging class of helical aromatics with unique topologies, called π-expanded helicenes,[7] which show not only angularly but also linearly *ortho*-annulated rings in a helical arrangement (Figure 1a). Technically, π-expanded helicenes are obtained by expanding the helicene framework with an additional rim(s) of fused rings and by removing afterwards the inner helicene rim(s). This π-expansion gives rise to helical structures with increasing diameters and higher flexibility, which together with the acene electronic structure of the linear segments in the aromatic framework, provide new features previously unseen in helical aromatics. Nevertheless, the synthesis of π-expanded helicenes is still in its infancy and, similarly to helicenes, remains very challenging because it requires the introduction of a certain degree of strain that simultaneously prevents their formation. For instance, to the best of our knowledge, multiple π-expanded helicenes are still undocumented.

Herein, we describe the synthesis of a series of nitrogenated benzodipentaphenes (**1**-**3**) constituted by 11 fused aromatic rings that extend between 2.2 and 2.6 nm in length (Figure 1c), one of which (**3**) shows a highly distorted aromatic backbone with an unprecedented double π-expanded helicene structure.

Benzodipentaphenes **1**-**3** are structural isomers that vary on the arrangement of their fused rings (Z-shaped or U-shaped). Benzodipentaphene **1** is almost planar because of the Z-Z arrangement of their fused rings, in which there is no steric interaction between the bulky triisopropylsilyl (TIPS) substituents. Conversely, benzodipentaphene **2** adopts a π-expanded helicene structure because of the Z-U arrangement of their fused rings that brings together two TIPS groups in the U segment. Lastly, benzodipentaphene **3** adopts a double π-expanded helicene structure with two half-helices of opposite turns because of the U-U arrangement of their fused rings that brings together two couples of TIPS groups. Remarkably, the steric effects between TIPS substituents in the U segments are

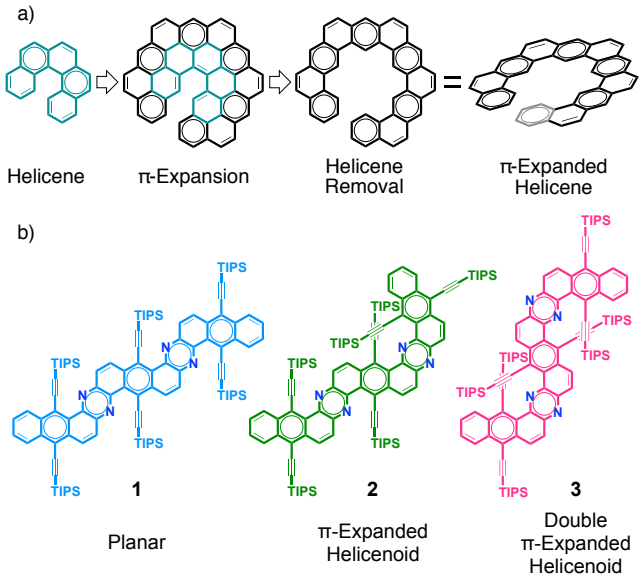

Figure 1. a) General structure of helicenes and π-expanded helicenes. b) The benzodipentaphene series reported in this work.

moderate enough to allow the synthesis of **3**, but also, large enough to introduce the strain necessary to induce the double π-expanded helicene structure. Structural, optoelectronic and electrochemical characterization, supported by theoretical calculations, reveal that benzodipentaphene **3**, despite its highly distorted aromatic backbone, is a highly conjugated polycyclic aromatic hydrocarbon with a high fluorescence quantum yield ($\Phi = 0.73$).

RESULTS AND DISCUSSION

Synthesis. Benzodipentaphenes **1-3** were obtained from the cyclocondensation reaction between diamine **4** and tetraone **5** (Scheme 1a). Experimental and characterization details are given in the supporting information. The precursor of diamine **4**, namely anthrathiadiazole **7**, was prepared from anthrathiadiazolequinone **6**[8] in one step. Anthracene-1,2,5,6-tetraone **5** was prepared from 2,6-dibromo-9,10-bis(triisopropylsilylethynyl)anthracene (**8**)[9] in three steps (Scheme 1b), which include a borylation-oxidation sequence, followed by the subsequent oxidation of the hydroxy groups of **10** into the desired tetraone **5**. Diamine **4** was generated by reduction of **7** by $LiAlH_4$ just before the reaction and was immediately allowed to react with tetraone **5** in a 1:2 mixture AcOH/$CHCl_3$ in refluxing conditions (Scheme 1a). Three structural isomers, namely, **1** (7%), **2** (11%) and **3** (2%), were isolated by column chromatography. Although the yield of **3** is very low, its formation is quite remarkable considering the higher strain that results from the steric interaction between two TIPS couples. Nevertheless, the low yield was not an issue to prepare sufficient amount for characterization, given the ability to prepare the precursors on a large scale.

Structure. The assigned structures of benzodipentaphenes **1-3** are consistent with ^{1}H-NMR, ^{13}C-NMR and high-resolution matrix-assisted-laser-desorption-ionization time-of-flight mass spectrometry (MALDI-TOF HRMS) characterization. Benzodipentaphene **2** with a single helical U segment was obtained as a mixture of *P*/*M* enantiomers. Meanwhile, benzodipentaphene **3** with two helical U segments can exist in the achiral (*P*,*M*) meso form or as a mixture of *P*,*P*/*M*,*M* enantiomers. Notably, only one isomer of benzodipentaphene **3**

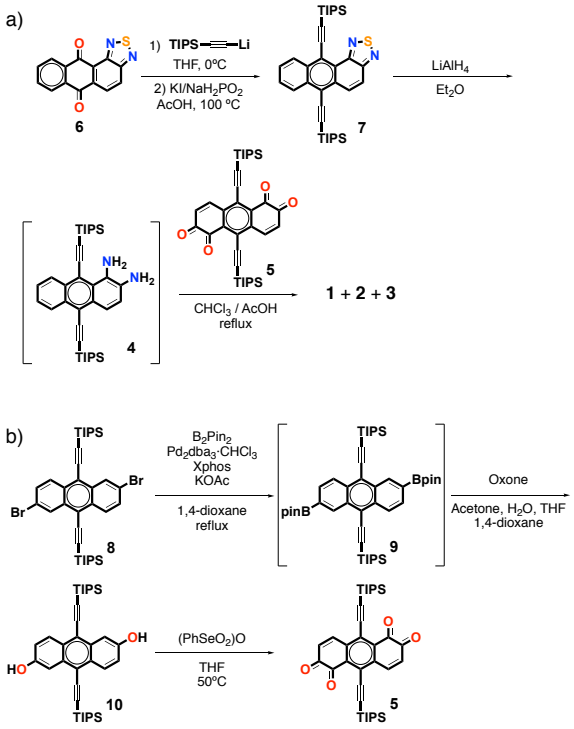

Scheme 1. Synthesis of benzodipentaphenes **1-3**.

was observed and isolated but it was not possible to assign its configuration spectroscopically. Single crystals were obtained for **1** and **3** by slow solvent evaporation from a $CHCl_3$ solution confirmed the structure **1** and allowed us to assign the structure of **3** (Figure 2) by X-ray diffraction. However, after several attempts, we were unable to obtain crystals of benzodipentaphene **2** suitable for X-ray diffraction and therefore the structure was calculated (Figure S1).

The crystal structure of benzodipentaphene **1** (Figures 2a and 2b) shows that the aromatic core is almost flat with small twists in the terminal ABC/A'B'C' segments (end-to-end twists of +12.0° and –12.0°, respectively) and along the BCD/B'C'D' (–10.1° and +10.1°, respectively) and the DEF/D'E'F' (+6.2° and –6.2°, respectively) bays.

The optimized geometry of benzodipentaphene **2** (Figure S1) shows a combined the structure of the Z and the U segments observed on the crystal structures of benzodipentaphenes **1** and **3** (Figure 2). The model illustrates that benzodipentaphene **2** adopts a planar structure along the Z segment similar to **1** and a π-expanded helicene structure in the U segment with dihedral angles consistent with those observed in the crystal structures of **3**.

The crystal structure of benzodipentaphene **3** confirms that the isolated isomer adopts a double π-expanded helicene structure with the achiral (*P*,*M*) meso form (Figures 2c and 2d). The aromatic core shows two half-helices with a diameter of 10.0 Å and an angle of 40.6° that change helicity in the F ring and that extend vertically along the perpendicular axis to the rings, and thus, the two terminal benzene rings (A and A') are in an almost parallel disposition at a distance (pitch) of 4.62 Å. Benzodipentaphene **3** combines both planar and twisted segments. For instance, the central anthracene EFE' segment is planar, while the terminal anthracene ABC/A'B'C' segments (end-to-end twist of –11.9° and +11.9°, respectively), and the two phenazine CDE/C'D'E' segments (end-to-end twist of

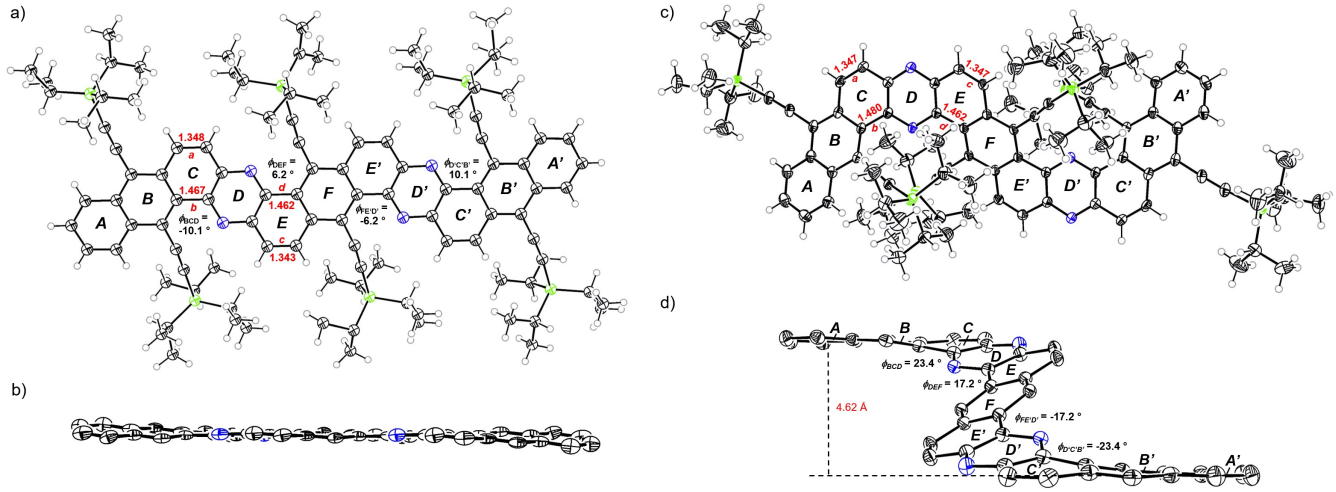

Figure 2. X-Ray crystal structures: a) top and b) side views of **1**; c) top and d) side views of **3** with selected bond lengths (in Å) and selected torsion angles. The thermal ellipsoids were scaled to 50% probability. Triisopropylsilylethynyl substituents and hydrogen atoms are omitted for clarity in side views.

+23.9° and –23.9°, respectively) are twisted. This highly distorted structure is due to the steric hindrance between the two couples of bulky TIPS groups in the inner rim of the U segments that increases the torsion angle along the BCD/B'C'D' (+23.4° and –23.4°, respectively) and the DEF/D'E'F' (+17.2° and –17.2°, respectively) bays.

Variable temperature ^{1}H-NMR (VT-NMR) experiments carried out on benzodipentaphene **3** in *o*-dichlorobenzene-d_4 show nearly invariable signals and no signs of coalescence with the increasing temperature (Figure S2). This indicates that **3** does not undergo any conformational change within the temperature range of the measurements (between 298 and 393 K).

Bond length analysis of the crystal structures of **1** and **3** provides fundamental information about the electronic structure. On the basis of this structural analysis, the dominant resonance structures of **1** and **3** is best represented by Clar's sextet rule with four K-regions with a double bond character (on C, E, E' and C' rings) and naphthalene (AB and A'B'), benzene (F) and pyrazine (D and D') groups. For instance,the average bond lengths of bonds a/c and b/d in rings C and E are ~1.35 and ~1.46 Å, respectively (Figure 2a and 2c), which are close to equivalent double (1.350 Å) and single (1.465 Å) bond lengths in the central ring in phenanthrene.[10] All other rings without angular annulations show bond lengths in the range of 1.36-1.43 Å that are close to the typical bond lengths observed in aromatic rings.

The bond lengths observed on the crystal structures are in good agreement with the geometries and with the local aromaticity – indicated by the nuclear independent chemical shift (NICS) values and by anisotropy of the induced current density (ACID) plots – calculated for benzodipentaphenes **1-3** at the B3LYP/6-311+G(d,p) level (Figures 3 and S3-S5). The largest NICS(0) values (between –6.2 and –8.2 ppm) were found on the naphthalene (AB and A'B'), benzene (F) and pyrazine (D and D') groups (the assignments correspond to the lettering shown in Figure 2), while lowest NICS(0) values (between –0.4 and –2.6 ppm) were found on the rings of the four K-regions (C, E, E' and C' rings), which is consistent with the aromatic character of each ring (Figures 3 and S4). ACID plots of benzodipentaphenes **1-3** (Figures 3 and S5) are consistent with NICS values showing a diamagnetic current in the periphery in all cases. This agrees with their aromatic nature and with a high degree of delocalization along the benzodipentaphene core.

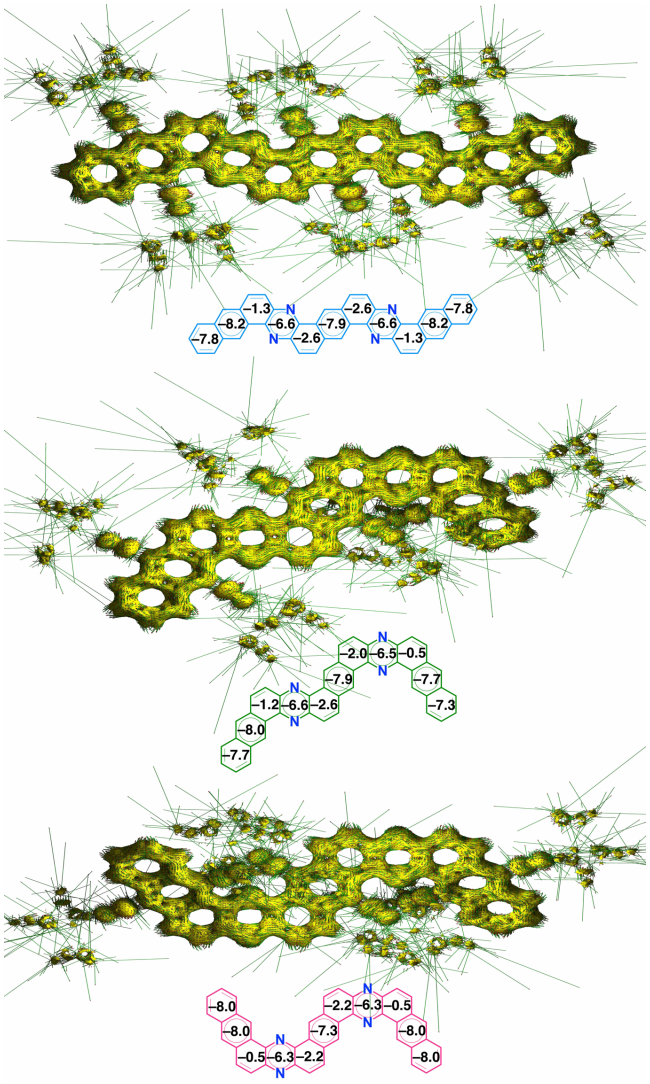

Figure 3. ACID plots and NICS(0) values for **1-3**.

Optoelectronic and redox properties. To shine light on the optoelectronic properties of benzodipentaphenes **1-3**, UV-vis electronic absorption spectra (Figure 4a) were recorded in toluene and CH_2Cl_2 yielding with similar results (Figure S6 and Table S1). Three sets of similar absorption bands can be identified in the 250-300, 300-475 and 475-550 nm regions, where the largest differences were observed in the 300-475 nm region. In the lowest energy 475-550 nm region, similar vibronically resolved absorption bands were observed that appear gradually red-shifted with the increasing helical nature of the aromatic core (λ_{max} = 523, 526 and 530 nm respectively for **1**, **2** and **3**). According to TD-DFT calculations, the longest-wavelength absorptions of **1** and **2** were attributed to a combination of the HOMO→LUMO (73% and 53%, respectively) and HOMO→LUMO+1 (23% and 41%, respectively) transitions, whereas the longest-wavelength absorption of **3** was-mainly attributed to the HOMO→LUMO+1 (93%) transition (Table S2).

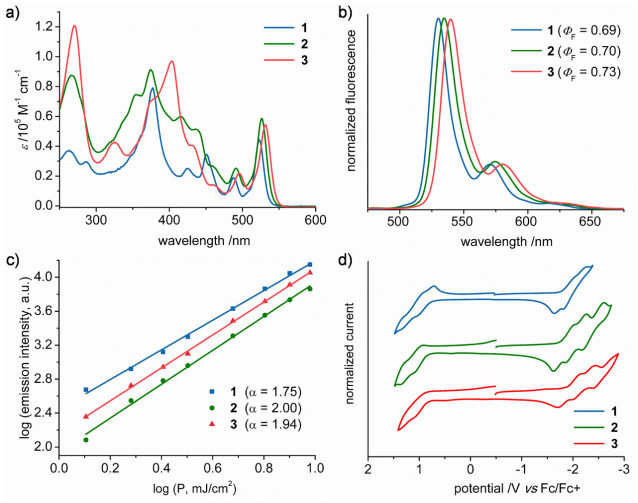

Figure 4. a) UV/Vis absorption and b) fluorescence spectra in CH_2Cl_2 (λ_{ex}= 450 nm). c) Power dependence of the two-photon-excited emission at 800 nm. d) Cyclic voltammograms in *o*-dichlorobenzene using nBu$_4$NPF$_6$ (0.05 M) as an electrolyte (potentials versus Fc/Fc$^+$). Scan rate: 100 mV/s.

Sharp and vibronically-resolved mirror-shaped fluorescence bands (Figure 4b and S6, Table S1) were observed in benzodipentaphenes **1-3**. The fluorescence bands appear gradually red-shifted with the increasing with the number of U (helical) segments in the aromatic core (λ_{em} = 523, 526 and 530 nm, respectively for **1**, **2** and **3**), in line with the electronic absorption spectra. Very high fluorescence quantum yields were observed, which remarkably tend to increase with the number of U (helical) segments (Φ = 0.69, 0.70 and 0.73, respectively for **1**, **2** and **3**). This is in contrast with previous observations in twisted aromatics that show how the distortion of the aromatic core reduces drastically their fluorescence quantum yields.[1g] The high quantum yields observed in benzodipentaphene **3** can be justified in terms of the extended π-conjugation of the LUMO,[11] which is not interrupted across the highly distorted aromatic framework (see Figures 3 and 5, and calculations below).

Given the extended conjugation and the high fluorescence quantum yields, the two-photon absorption (TPA) and emission properties of these compounds was investigated. To this end, an 800 nm femtosecond laser was employed as the excitation source and the two-photon up-conversion process was evaluated by measuring input power intensity dependent changes upon excitation wavelength (Figure 4c). For all the compounds, the slopes of the logarithmic plot of fluorescence output with excitation intensity (α = 1.75, 2.00 and 1.94, respectively for **1**, **2** and **3**) evidenced a two-photon absorption process in all cases. The emission spectra induced by excitation with two 800 nm photons of is exactly coincident with the one induced by a single 450 nm photon (Figure S7). The TPA cross-section at 800 nm for benzodipentaphenes **1-3** was estimated to be 374, 182 and 212 GM, respectively. These values are comparable to those reported for extended π-conjugated systems.[2e,12]

The electrochemical properties were investigated by cyclic voltammetry measurements in *o*-dichlorobenzene using nBu$_4$NPF$_6$ as the electrolyte (Figure 4d and Table S3). The voltammograms show in all cases a set of reduction and a set of oxidation processes within the solvent-supported electrolyte window. The planar benzodipentaphene **1** showed two reductions and two oxidations processes, the π-expanded helicenoid **2** showed three reduction and two oxidation processes, while the double π-expanded helicenoid **3** showed three reduction and one oxidation processes. From the oxidation and reduction potentials of benzodipentaphenes **1-3**, it can be concluded that the redox properties vary with the number of U (helical) segments present in the aromatic core.

The optoelectronic and electrochemical characterization allowed to estimate the energy levels for the benzodipentaphenes **1-3** (Tables S1 and S3) The optical HOMO LUMO gaps (E_g) were estimated from the onset of the absorption spectra. The E_g values of benzodipentaphenes **1-3** were very similar in all cases (2.31, 2.29 and 2.27 eV, respectively) but show how the gap slightly decreases as the aromatic core with the increasing number of U (helical) segments, this trend is also observed in the calculated E_g values (Table S4). Similarly, the electrochemical LUMO levels or electron affinities (E_{LUMO}) were estimated from the onset potentials of the first reduction peaks. The E_{LUMO} values of benzodipentaphenes **1-3** were again very similar (–3.06, –3.04 and –2.96 eV, respectively) and tend to decrease slightly with the increasing number of U (helical) segments, this trend is also observed in the calculated E_{LUMO} values (Table S4). Both HOMO and LUMO (B3LYP-6-31g(d,p)) are highly delocalized along the benzodipentaphene core (Figure 5). The HOMOs electronic density resembles the HOMOs of three individual 9,10-bis(ethynyl)anthracene (Figure S8), as the linking nitrogen atoms show negligible electronic density. In contrast, the LUMOs show a large electronic density that spans all over the aromatic core except in the non-terminal K-regions, where there is reduced electronic density if any. The frontier orbitals shape and spatial distribution is nearly the same in both Z- and U-shaped segments. This agrees with the above-mentioned ACID plots that shows diamagnetic currents that run around the periphery of the benzodipentaphene core (Figure 3).

CONCLUSIONS

To conclude, we have reported here a series of sterically congested nitrogenated benzodipentaphenes, which reach 2.6 nm in length, constituted of Z- and/or U-shaped segments. The Z-shaped segments are planar because of the lack of intramolecular steric interactions, while the U-shaped segments show

a π-expanded helicene structure as an effect of the strain introduced by the steric interactions between TIPS groups. Benzodipentaphene **3** with two U segments adopts a highly distorted double π-expanded helicene structure (diameter = 10.0 Å, pitch = 4.6 Å, angle = 40.6°) with two half-helices of opposite turns, as illustrated by X-ray crystallography. Optoelectronic and electrochemical characterization shows that the number of U-shaped (helical) segments in the aromatic core redshifts both electronic absorption and fluorescence and varies the redox properties. Remarkably, benzodipentaphene **3** shows a high fluorescence quantum yield (Φ = 0.73) despite its highly distorted aromatic backbone, which is a prerequisite for developing light-emitting applications. Overall this works describes the synthesis of a novel and unprecedented member of the family of π-expanded helicenes and describes a set of fundamental properties that shines light on the structural factors that govern the properties of non-planar aromatics.

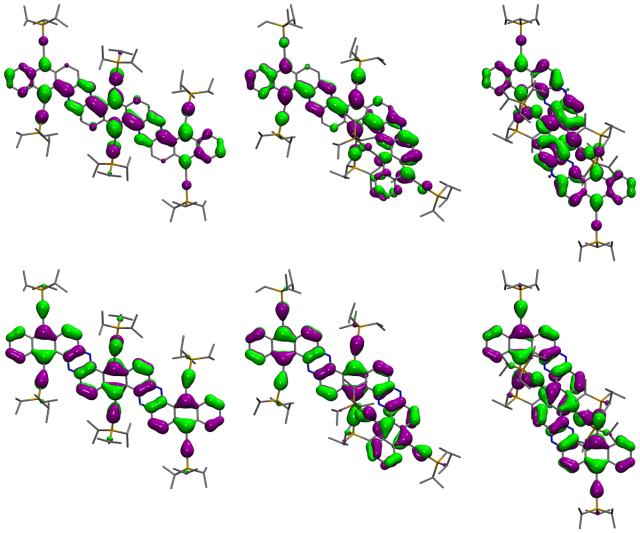

Figure 5. LUMO (top) and HOMO (bottom) orbitals at the B3LYP-6-31g(d,p) level for **1**, **2** and **3** from left to right.

ASSOCIATED CONTENT

Supporting Information

The Supporting Information is available free of charge on the ACS Publications website. Full synthetic and characterization procedures (PDF) and crystal structures of **1** and **3** (CIF).

AUTHOR INFORMATION

Corresponding Author

* amateo@polymat.eu

Author Contributions

The manuscript was written through contributions of all authors, who have given approval to the final version of the manuscript.

ACKNOWLEDGMENT

A.M.-A. acknowledge support of the Basque Science Foundation for Science (Ikerbasque), POLYMAT, the University of the Basque Country (Grupo de Investigación GIU17/054), Gobierno Vasco (PIBA 2019-09 and BERC program) and Gobierno de España (Ministerio de Economía y Competitividad CTQ2016-77970-R) and thank for technical and human support provided by SGIker of UPV/EHU and European funding (ERDF and ESF). F.C. and A. M.-A acknowledge that this project has received funding from the European Union's Horizon 2020 research and innovation programme under the Marie Skłodowska-Curie grant agreement No 839626. F.C. and A.M.-A. acknowledge that this project has received funding from the European Research Council (ERC) under the European Union's Horizon 2020 research and innovation programme (grant agreement n° 722951). A. S acknowledges the support of Japan Society for the Promotion of Science (JSPS) with the KAKENHI Grant-in-Aid for Scientific Research (A) (Grant No. JP16H02285). M.M.-F. acknowledges support from the Portuguese Foundation for Science and Technology (FCT), under the project IF/00894/2015, and the project CICECO-Aveiro Institute of Materials, FCT Ref. UID/CTM/50011/2019, UIDB/50011/2020 & UIDP/50011/2020, financed by national funds through the FCT/MEC and when appropriate co-financed by FEDER under the PT2020 Partnership Agreement.

REFERENCES

(1) (a) Petrukhina, M. A.; Scott, L. T.; Kroto, H. W. *Fragments of Fullerenes and Carbon Nanotubes: Designed Synthesis, Unusual Reactions, and Coordination Chemistry*; Wiley, 2011; (b) Ball, M.; Zhong, Y.; Wu, Y.; Schenck, C.; Ng, F.; Steigerwald, M.; Xiao, S.; Nuckolls, C. *Acc. Chem. Res.* **2015**, *48*, 267; (c) Segawa, Y.; Yagi, A.; Matsui, K.; Itami, K. *Angew. Chem. Int. Ed.* **2016**, *55*, 5136; (d) Pun, S. H.; Miao, Q. *Acc. Chem. Res.* **2018**, *51*, 1630; (e) Majewski, M. A.; Stępień, M. *Angew. Chem. Int. Ed.* **2019**, *58*, 86; (f) Pascal, R. A. *Chem. Rev.* **2006**, *106*, 4809; (g) Bedi, A.; Gidron, O. *Acc. Chem. Res.* **2019**, *52*, 2482; (h) Shen, Y.; Chen, C.-F. *Chem. Rev.* **2012**, *112*, 1463; (i) Gingras, M. *Chem. Soc. Rev.* **2013**, *42*, 1051; (j) Rickhaus, M.; Mayor, M.; Juríček, M. *Chem. Soc. Rev.* **2016**, *45*, 1542; (k) Mateo-Alonso, A. *Eur. J. Org. Chem.* **2017**, *2017*, 7006.

(2) (a) Nakakuki, Y.; Hirose, T.; Sotome, H.; Miyasaka, H.; Matsuda, K. *J. Am. Chem. Soc.* **2018**, *140*, 4317; (b) Evans, P. J.; Ouyang, J.; Favereau, L.; Crassous, J.; Fernández, I.; Perles, J.; Martín, N. *Angew. Chem. Int. Ed.* **2018**, *57*, 6774; (c) Reger, D.; Haines, P.; Heinemann, F. W.; Guldi, D. M.; Jux, N. *Angew. Chem. Int. Ed.* **2018**, *57*, 5938; (d) Cruz, C. M.; Castro-Fernández, S.; Maçôas, E.; Cuerva, J. M.; Campaña, A. G. *Angew. Chem. Int. Ed.* **2018**, *57*, 14782; (e) Cruz, C. M.; Marquez, I. R.; Mariz, I. F. A.; Blanco, V.; Sanchez-Sanchez, C.; Sobrado, J. M.; Martin-Gago, J. A.; Cuerva, J. M.; Macoas, E.; Campana, A. G. *Chem. Sci.* **2018**, *9*, 3917; (f) Ma, J.; Fu, Y.; Dmitrieva, E.; Liu, F.; Komber, H.; Hennersdorf, F.; Popov, A. A.; Weigand, J. J.; Liu, J.; Feng, X. *Angew. Chem. Int. Ed.* **2020**, DOI: 10.1002/anie.201914716; (g) Nakamura, K.; Furumi, S.; Takeuchi, M.; Shibuya, T.; Tanaka, K. *J. Am. Chem. Soc.* **2014**, *136*, 5555; (h) Fujikawa, T.; Segawa, Y.; Itami, K. *J. Am. Chem. Soc.* **2015**, *137*, 7763; (i) Hu, Y.; Wang, X.-Y.; Peng, P.-X.; Wang, X.-C.; Cao, X.-Y.; Feng, X.; Müllen, K.; Narita, A. *Angew. Chem. Int. Ed.* **2017**, *56*, 3374; (j) Wang, X.-Y.; Wang, X.-C.; Narita, A.; Wagner, M.; Cao, X.-Y.; Feng, X.; Müllen, K. *J. Am. Chem. Soc.* **2016**, *138*, 12783; (k) Hu, Y.; Paternò, G. M.; Wang, X.-Y.; Wang, X.-C.; Guizzardi, M.; Chen, Q.; Schollmeyer, D.; Cao, X.-Y.; Cerullo, G.; Scotognella, F.; Müllen, K.; Narita, A. *J. Am. Chem. Soc.* **2019**, *141*, 12797; (l) Ferreira, M.; Naulet, G.; Gallardo, H.; Dechambenoit, P.; Bock, H.; Durola, F. *Angew. Chem. Int. Ed.* **2017**, *56*, 3379; (m) Zhao, K.; Long, G.; Liu, W.; Li, D.-S.; Gao, W.; Zhang, Q. *J. Org. Chem.* **2020**, *85*, 291; (n) Schuster, N. J.; Paley, D. W.; Jockusch, S.; Ng, F.; Steigerwald, M. L.; Nuckolls, C. *Angew. Chem. Int. Ed.* **2016**, *55*, 13519; (o) Schuster, N. J.; Hernández Sánchez, R.; Bukharina, D.; Kotov, N. A.; Berova, N.; Ng, F.; Steigerwald, M. L.; Nuckolls, C. *J. Am. Chem. Soc.* **2018**, *140*, 6235; (p) Daigle, M.; Miao, D.; Lucotti, A.; Tommasini, M.; Morin, J.-F. *Angew. Chem. Int. Ed.* **2017**, *56*, 6213; (q) Han, S.; Bond, A. D.; Disch, R. L.; Holmes, D.; Schulman, J. M.; Teat, S. J.; Vollhardt, K. P. C.; Whitener, G. D. *Angew. Chem. Int. Ed.* **2002**, *41*, 3223; (r) Han, S.; Anderson, D. R.; Bond, A. D.; Chu, H. V.; Disch, R. L.; Holmes, D.; Schulman, J. M.; Teat, S. J.; Vollhardt, K. P. C.; Whitener, G. D. *Angew. Chem. Int. Ed.* **2002**, *41*, 3227.

(3) (a) Sawada, Y.; Furumi, S.; Takai, A.; Takeuchi, M.; Noguchi, K.; Tanaka, K. *J. Am. Chem. Soc.* **2012**, *134*, 4080; (b) Cruz, C. M.; Márquez, I. R.; Castro-Fernández, S.; Cuerva, J. M.; Maçôas, E.; Campaña, A. G. *Angew. Chem. Int. Ed.* **2019**, *131*, 8152; (c) Otani, T.; Tsuyuki, A.; Iwachi, T.; Someya, S.; Tateno, K.; Kawai, H.; Saito, T.; Kanyiva, K. S.; Shibata, T. *Angew. Chem. Int. Ed.* **2017**, *56*, 3906; (d) Yang, Y.; da Costa,

R. C.; Fuchter, M. J.; Campbell, A. J. *Nat. Photonics* **2013**, *7*, 634; (e) Brandt, J. R.; Salerno, F.; Fuchter, M. J. *Nat. Rev. Chem.* **2017**, *1*, 0045.
(4) Verbiest, T.; Elshocht, S. V.; Kauranen, M.; Hellemans, L.; Snauwaert, J.; Nuckolls, C.; Katz, T. J.; Persoons, A. *Science* **1998**, *282*, 913.
(5) (a) Liu, G.; Xiao, C.; Negri, F.; Li, Y.; Wang, Z. *Angew. Chem. Int. Ed.* **2020**, *59*, 2008; (b) Zhong, Y.; Kumar, B.; Oh, S.; Trinh, M. T.; Wu, Y.; Elbert, K.; Li, P.; Zhu, X.; Xiao, S.; Ng, F.; Steigerwald, M. L.; Nuckolls, C. *J. Am. Chem. Soc.* **2014**, *136*, 8122.
(6) (a) Naaman, R.; Waldeck, D. H. *J. Phys. Chem. Lett.* **2012**, *3*, 2178; (b) Kiran, V.; Mathew, S. P.; Cohen, S. R.; Hernandez Delgado, I.; Lacour, J.; Naaman, R. *Adv. Mater.* **2016**, *28*, 1957.
(7) (a) Kiel, G. R.; Patel, S. C.; Smith, P. W.; Levine, D. S.; Tilley, T. D. *J. Am. Chem. Soc.* **2017**, *139*, 18456; (b) Nakakuki, Y.; Hirose, T.; Matsuda, K. *J. Am. Chem. Soc.* **2018**, *140*, 15461.
(8) Huang, H. S.; Chen, T. C.; Chen, R. H.; Huang, K. F.; Huang, F. C.; Jhan, J. R.; Chen, C. L.; Lee, C. C.; Lo, Y.; Lin, J. J. *Bioorg. Med. Chem.* **2009**, *17*, 7418.
(9) (a) Park, J. H.; Chung, D. S.; Park, J. W.; Ahn, T.; Kong, H.; Jung, Y. K.; Lee, J.; Yi, M. H.; Park, C. E.; Kwon, S. K.; Shim, H. K. *Org. Lett.* **2007**, *9*, 2573; (b) Zippel, S.; Boldt, P. *Synthesis* **1997**, *1997*, 173.
(10) Herndon, W. C. *J. Am. Chem. Soc.* **1974**, *96*, 7605.
(11) Yamaguchi, Y.; Matsubara, Y.; Ochi, T.; Wakamiya, T.; Yoshida, Z.-i. *J. Am. Chem. Soc.* **2008**, *130*, 13867.
(12) Cai, Z.; Vázquez, R. J.; Zhao, D.; Li, L.; Lo, W.-y.; Zhang, N.; Wu, Q.; Keller, B.; Eshun, A.; Abeyasinghe, N.; Banaszak-Holl, H.; Goodson, T.; Yu, L. *Chem. Mater.* **2017**, *29*, 6726.